

Microscopic analysis of quasielastic scattering and breakup reactions of neutron-rich nuclei $^{12,14}\text{Be}$

V. K. Lukyanov,¹ D. N. Kadrev,² E. V. Zemlyanaya,¹ K. V. Lukyanov,¹ A. N. Antonov,² and M. K. Gaidarov²

¹*Joint Institute for Nuclear Research, Dubna 141980, Russia*

²*Institute for Nuclear Research and Nuclear Energy,
Bulgarian Academy of Sciences, Sofia 1784, Bulgaria*

A microscopic analysis of the optical potentials (OPs) and cross sections of quasielastic scattering of $^{12,14}\text{Be}$ on ^{12}C at 56 MeV/nucleon and on protons at energy near 700 MeV is carried out. For lower energy scattering the real part of the OP is calculated by using of double-folding procedure accounting for the anti-symmetrization effects, while the imaginary part is obtained on the base of the high-energy approximation (HEA). The HEA is also applied to the calculations of both real and imaginary OPs when solving the relativistic equation for the high-energy proton-nucleus elastic scattering. The neutron and proton density distributions computed in different microscopic models for ^{12}Be and ^{14}Be are used. In the present hybrid model of the optical potential the only free parameters are the depths of the real and imaginary parts of OP obtained by fitting the experimental data. The role of the inelastic scattering channel to the first excited 2^+ and 3^- states in ^{12}C when calculating the quasielastic cross sections, as well as the modified density of the ^{12}C target accounting for the surface effects are studied. In addition, the cluster model, in which ^{14}Be consists of a $2n$ -halo and the ^{12}Be core, is applied to calculate the cross sections of diffraction breakup and stripping reactions in $^{14}\text{Be}+^{12}\text{C}$ scattering and longitudinal momentum distributions of ^{12}Be fragments at energy of 56 MeV/nucleon. A good agreement of the theoretical results with the available experimental data of both quasielastic scattering and breakup processes is obtained.

PACS numbers: 25.40.Cm, 24.10.Ht, 25.60.Gc, 21.10.Gv

I. INTRODUCTION

Since the pioneering works of Tanihata *et. al.* [1, 2] the study of halo nuclei has attracted much attention. Halo nuclei are commonly considered to have a compact nuclear core and a few valence nucleons surrounding the core. Characteristic features displayed by these nuclei include weak binding energy of the valence nucleons, narrow momentum distributions of the reaction products due to the fragmentation and the anomalously large interaction cross section.

The microscopic studies of elastic scattering of $^{6,8}\text{He}$, ^{11}Li , $^{10,11}\text{Be}$, and ^8B on protons and nuclei and breakup processes performed in our previous works [3–8] have confirmed the specific internal spatial structure of these neutron- and proton-halo nuclei and shed light on the relative contributions of different reaction mechanisms. Studying this series of light nuclei, the interest of considering very neutron-rich beryllium isotopes is provoked, for instance, by the magicity loss for the $N = 8$ nucleus ^{12}Be [9–13] and the halo structure of ^{14}Be nucleus, which is located at the neutron drip line and its two-neutron separation energy is $S_{2n} = 1.26(13)$ MeV [14]. ^{14}Be is a Borromean nucleus like ^{11}Li and it has a two-neutron halo structure with a ^{12}Be core plus two loosely-bound neutrons [15–19].

Here we note that the task for the structure of the two-neutron halo nuclei is of important interest in connection with the general question about the behavior of the dineutron ($2n$) formations in exotic nuclei. First, we note the work of Migdal [20], in which it was shown that the attractive force between two neutrons (itself too

weak to form a bound $2n$ system) in the presence of a nucleus (itself unable to bind a single neutron) may lead to a bound state of the three particles, i.e. it is a dineutron coupled to a nuclear core (see also studies, e.g., in Refs. [21–26]). The possibility that cluster states more complex than dineutrons may exist has been pointed also in Ref. [20].

The interest to $2n$ -formations has increased also in relation to the experiments that showed a ground state dineutron decay of ^{16}Be nucleus [27]. It has been observed there a small angle of emission between two neutrons and a value of the two-neutron separation energy $S_{2n} = 1.35(10)$ MeV has been measured. Here we note that in the case of the ^{14}Be nucleus this energy ($S_{2n} = 1.26$ MeV) is close to that in ^{16}Be .

As noted in Ref. [16], the ^{14}Be system is even more interesting than ^{11}Li since the wave function of the last two neutrons in ^{14}Be is expected to contain a larger $(2s_{1/2})^2$ shell-model component. In addition, the two-neutron separation energy in ^{14}Be is much larger than that of ^{11}Li ($S_{2n} = 0.376$ MeV). So, it is of interest to study this effect of extra binding on the properties of the neutron halo (see also Ref. [28]). At the same time, however, one must bear in mind the relatively small difference between the halo rms radii of both nuclei (6 fm in ^{11}Li [29] and 5.5 fm in ^{14}Be [1, 2, 15]). All the mentioned facts give a reason for more detailed studies of these neutron-rich systems with a $2n$ -halo and their interactions with nuclei.

Many experimental and theoretical studies of the matter density distributions in nuclei far from stability show an extended low-density tail at large radial distances in their behavior. As an example, the calculations in the

framework of the relativistic Hartree-Bogoliubov model have predicted very large neutron skin in ^{14}Be and a large prolate deformation of this nucleus [30]. Besides, the related with the matter densities extraordinarily large radii (see, for instance, Ref. [31, 32]) are in favor of the halo structure of the neutron(proton)-rich nuclei.

From the analyses of proton elastic scattering in inverse kinematics at intermediate energy about 700 MeV/nucleon Ilieva *et al.* [21] showed an extended matter distribution for $^{12,14}\text{Be}$ nuclei. A clear evidence of a halo structure has been obtained demonstrating better qualitative description of the p - ^{14}Be cross section when the ^{14}Be nucleus is supposed to consist of a ^{12}Be core and two halo neutrons rather than a ^{10}Be core plus four valence neutrons. Several phenomenological parametrizations including the symmetrized Fermi function, as well as a sum of Gaussian ones, were used for the nuclear-matter density distribution in the analysis performed in Ref. [21].

The ground-state proton, neutron, and matter densities, the corresponding root-mean-square (rms) radii and elastic charge form factors of ^{12}Be and ^{14}Be nuclei have been studied through shell-model calculations using different model spaces for the core and the extra two halo neutrons [33] and in a three-body model of (core+ $n+n$), where the core and halo density distributions were described by the single-particle wave functions of the Woods-Saxon (WS) potential [28]. A renormalized zero-range version of the same three-body model has been applied to study the rms radii of weakly-bound light nuclei (^6He , ^{11}Li , ^{14}Be , and ^{20}C), particularly the mean square distance between the two neutrons forming halo in them [34]. The good qualitative agreement between the recently measured data and the theoretical results has indicated that the model is reasonable for ^{14}Be validating the large probability of the halo neutrons to be found outside the interaction range. Under the assumption of similar decomposition of the matter density with core and halo contributions, in Ref. [35] simple analytic expressions for nuclear densities with a correct asymptotic behavior were proposed for exotic nuclei including the 7 - ^{14}Be isotopes.

A "long tail" of neutron density distribution compared with the proton density distribution in ^{14}Be nucleus based on the relativistic mean-field (RMF) theory has been displayed in Ref. [36]. It was shown in Ref. [37] that the density-dependent RMF formalism can satisfactorily reproduce the experimental data of the abnormally large rms radius of ^{14}Be , in which the halo neutrons occupy the already mentioned above $2s_{1/2}$ level instead of the $1d_{5/2}$ level. On the contrary, the dominance of the d -configuration in the $N = 8$ shell in ^{12}Be was strongly revealed from the breakup reaction on a proton target at intermediate energy [38]. Also, different measurements of reaction cross sections of ^{14}Be on protons and carbon target at about 41 and 76 MeV/nucleon [39], on Be, C, and Al targets at several energies in the range of 45–120 MeV/nucleon [40], as well as at relativistic energies [41],

allowed one to deduce the matter density distribution of this two-neutron halo nucleus supporting the s -wave dominance in the ground-state density of ^{14}Be . The fact that the ground-state wave function of ^{14}Be includes a strong $2s_{1/2}$ admixture has been confirmed in the experiment of Labiche *et al.* [42], in which they studied the dissociation of ^{14}Be at 35 MeV/nucleon on carbon and lead targets in a kinematically complete measurement. Here we would like to mention the result for ^{14}Be nucleus from more sophisticated microscopic calculations within the three-cluster generator coordinate method (GCM) [43] involving the ones for the proton and neutron densities of $^{12,14}\text{Be}$.

The widths of the measured momentum distributions following the fragmentation of $^{12,14}\text{Be}$ on ^{12}C at incident energies of 56 and 65 MeV/nucleon have offered a clear qualitative signature of the spatial distribution of the halo particles [16, 44]. The deduced value (92.2 ± 2.7 MeV/c) of the width parameter of the Lorentzian momentum distribution that describes the measured ^{12}Be longitudinal momentum distribution at 56 MeV/nucleon via the telescope method and the full width at half maximum (FWHM) equal to 95.6 ± 4.2 MeV/c of the single Gaussian that fits the distribution at 65 MeV/nucleon obtained via the spectrograph method were shown to be in agreement with the "neutron halo" structure of ^{14}Be . The direct fragmentation model has been applied in Ref. [45] to calculate both longitudinal and transverse momentum distributions of the ^{12}Be fragments emitted in ^{14}Be induced breakup reactions on ^{208}Pb and ^{12}C targets at beam energy of 56 MeV/nucleon and the results for the widths are very similar to the data of Zahar *et al.* [16].

In the earlier works (e.g., Refs. [46, 47]) the quasielastic scattering cross sections of $^{12,14}\text{Be}$ on ^{12}C at 56 MeV/nucleon laboratory incident energy have been calculated using phenomenological OPs of volume Woods-Saxon shapes plus surface terms (normalized derivative of WS volume terms) for both real (ReOP) and imaginary (ImOP) parts. In Ref. [46] for the case of $^{12}\text{Be}+^{12}\text{C}$ scattering such an additional real surface potential was not included. A substantial difference is seen from the comparison of the values of the ReOP and ImOP depths in both analyses [46, 47]. For instance, to obtain a good fit of the experimental $^{12,14}\text{Be}$ angular distributions the volume real potentials in [46] turned out twice deeper than the corresponding ones shown in Ref. [47]. At the same time the difference between the values of the volume imaginary potentials is even larger. This is the reason for the different total reaction cross sections σ_R (1238 mb and 1900 mb for ^{12}Be and ^{14}Be projectiles, respectively, in Ref. [46] and 911 mb and 1123 mb in Ref. [47]). The obtained in Ref. [47] values of σ_R fit better the experimentally measured values by Tanihata *et al.* [15] (927 mb and 1139 mb, respectively).

Recently, proximity potentials as an alternative way to produce the ReOP have been applied in the analysis of scattering cross sections of Be isotopes [48]. How-

ever, Woods-Saxon potential is used for the imaginary part of the OP. The first-order Dirac OP with direct and exchange parts and relativistic impulse approximation from Ref. [36] have been applied in Ref. [49] to calculate the cross sections of the elastic scattering of protons at $E_{lab} = 100$ and 200 MeV on ^{14}Be and on stable ^{12}C and ^{16}O nuclei. It has been concluded that the halo neutrons in ^{14}Be have effects only in small angular region $4^\circ < \theta < 11^\circ$. A step ahead in constructing nucleus-nucleus potentials was made very recently in Ref. [50] by using the double-folding method based on local chiral effective field theory interactions for the ^{16}O - ^{16}O system.

In our present work we aim to perform a fully microscopic analysis of quasielastic scattering and breakup reactions of neutron-rich nuclei $^{12,14}\text{Be}$. The hybrid model of OP [51, 52], which has been successfully applied before in our papers [3–8], is used to analyze the existing data of processes with $^{12,14}\text{Be}$ isotopes at incident energies $E < 100$ MeV/nucleon ($^{12,14}\text{Be}+^{12}\text{C}$ quasielastic scattering) [16, 46, 47] up to relativistic energy of 700 MeV ($p+^{12,14}\text{Be}$ elastic scattering) [21]. In the folding procedure the ReOP consists of both direct and exchange potentials with the isoscalar and isovector parts included. We use the effective nucleon-nucleon potential from Ref. [53] (see also [54]) and microscopic density distributions for ^{12}Be obtained within the variational Monte Carlo (VMC) model [55] and the generator coordinate method [43]. For ^{14}Be only the available GCM density [43] is used. The ImOP is obtained within the HEA model [56, 57], where the known parametrization of the elementary nucleon-nucleon (NN) cross section and scattering amplitude at $\theta = 0^\circ$ are used. In contrast to the analyses of quasielastic $^{12,14}\text{Be}$ on ^{12}C performed in Refs. [46, 47] with large number of optical model fitting parameters, the only free parameters in our model are the depths of the real and imaginary parts of the microscopic OP obtained by fitting the experimental differential cross section data.

We also search for other effects that should be incorporated in the microscopic study, namely, to account for the inelastic scattering to the low-lying 2^+ and 3^- collective states in ^{12}C in the quasielastic process and the role of the density distribution of the ^{12}C target with inclusion of surface terms. Such an investigation is supposed to figure out the role of the neutron halo for both Be projectiles. Second, in addition to the analysis of quasielastic scattering cross sections, we estimate important characteristics of the reactions with ^{14}Be , such as the breakup cross sections for the diffraction and stripping processes and the momentum distributions of ^{12}Be fragments from the breakup reaction $^{14}\text{Be}+^{12}\text{C}$ for which experimental data are available [16]. Such a complex study based on the microscopic method to obtain the OPs with a minimal number of free parameters and by testing density distributions of $^{12,14}\text{Be}$ which reflect their two-neutron halo structure would lead to a better understanding the structure of these neutron-rich nuclei and to a reduction of the inconsistency of describing the available data.

The structure of the paper is as follows. The theoretical scheme to calculate microscopically within the hybrid model the ReOP and the ImOP, as well as the results for the $^{12,14}\text{Be}+^{12}\text{C}$ quasielastic- and $p+^{12,14}\text{Be}$ elastic-scattering differential cross sections are presented in Sec. II. Section III contains the basic formulae to estimate the ^{14}Be breakup on ^{12}C in the stripping and diffraction processes within the cluster model with two-neutrons halo of ^{14}Be and the corresponding results for the longitudinal momentum distributions of ^{12}Be fragments. The summary and conclusions of the work are given in Sec. IV.

II. QUASIELASTIC SCATTERING OF $^{12,14}\text{Be}$ ON ^{12}C AND PROTONS

A. Hybrid model for the optical potential

The microscopic OP used in our calculations of quasielastic scattering differential cross sections contains the volume real part (V^F) including both the direct and exchange terms and the HEA microscopically calculated imaginary part (W^H). It has the form

$$U(r) = N_R V^F(r) + i N_I W^H(r). \quad (1)$$

The parameters N_R and N_I entering Eq. (1) renormalize the strength of OP and are fitted by comparison with the experimental cross sections.

The real part V^F realized numerically in [54] consists of the direct (V^D) and exchange (V^{EX}) single(double)-folding integrals that include effective NN potentials and density distribution functions of colliding nuclei. The V^D and V^{EX} parts of the ReOP have isoscalar (IS) and isovector (IV) contributions. The IS ones of both terms are:

$$V_{IS}^D(r) = \int d^3r_p d^3r_t \rho_p(\mathbf{r}_p) \rho_t(\mathbf{r}_t) v_{NN}^D(s), \quad (2)$$

$$V_{IS}^{EX}(r) = \int d^3r_p d^3r_t \rho_p(\mathbf{r}_p, \mathbf{r}_p + \mathbf{s}) \rho_t(\mathbf{r}_t, \mathbf{r}_t - \mathbf{s}) \times v_{NN}^{EX}(s) \exp\left[\frac{i\mathbf{K}(r) \cdot \mathbf{s}}{M}\right], \quad (3)$$

where $\mathbf{s} = \mathbf{r} + \mathbf{r}_t - \mathbf{r}_p$ is the vector between two nucleons, one of which belongs to the projectile and another one to the target nucleus. In Eq. (2) $\rho_p(\mathbf{r}_p)$ and $\rho_t(\mathbf{r}_t)$ are the densities of the projectile and the target, respectively, while in Eq. (3) $\rho_p(\mathbf{r}_p, \mathbf{r}_p + \mathbf{s})$ and $\rho_t(\mathbf{r}_t, \mathbf{r}_t - \mathbf{s})$ are the density matrices for the projectile and the target that are usually taken in an approximate form [58, 59] (see also Refs. [3, 4]). The effective NN interactions v_{NN}^D and v_{NN}^{EX} have their IS and IV components in the form of M3Y interaction obtained within g -matrix calculations using the Paris NN potential [53]. The expressions for the energy and density dependence of the effective NN

interaction are given, e.g., in Ref. [7]. In Eq. (3) $\mathbf{K}(r)$ is the local momentum of the nucleus-nucleus relative motion:

$$K(r) = \left\{ \frac{2Mm}{\hbar^2} [E - V^F(r) - V_c(r)] \right\}^{1/2} \quad (4)$$

with $M = A_p A_t / (A_p + A_t)$, where A_p , A_t , m are the projectile and target atomic numbers and the nucleon mass. As can be seen, $K(r)$ depends on the folding potential $V^F(r)$ that has to be calculated itself and, thus, nonlinearity effects occur as typical ingredients of the model and they have to be taken carefully into account.

Concerning the ImOP, it corresponds to the full microscopic OP derived in Refs. [51, 52, 60] within the HEA [56, 57]:

$$U^H = V_H(r) + iW^H(r) = -\frac{\hbar v}{(2\pi)^2} \bar{\sigma}_N (\bar{\alpha} + i) \times \int_0^\infty j_0(qr) \rho_p(q) \rho_t(q) f_N(q) q^2 dq. \quad (5)$$

In Eq. (5) $\rho(q)$ are the corresponding form factors of the nuclear densities, $\bar{\alpha}$ is the ratio of the real to imaginary part of the NN scattering amplitude at forward angles, $f_N(q) = \exp(-\beta q^2/2)$ is the q -dependence of the NN scattering amplitude and $\bar{\sigma}_N$ is the total NN scattering cross section that has been parametrized as function of the energy up to 1 GeV [61–63]. The values of $\bar{\alpha}$, $\bar{\sigma}_N$, and $\bar{\beta}$ are averaged over the isospin of the nucleus.

B. Results of calculations of cross sections

We calculate the OP [Eq. (1)] and the elastic scattering cross sections of $^{12,14}\text{Be}$ on ^{12}C and protons using the DWUCK4 code [64] for solving the Schrödinger equation. All the scattering cross sections will be shown in the figures as ratios to the Rutherford cross sections ($d\sigma/d\sigma_R$).

Concerning the beryllium $^{12,14}\text{Be}$ isotopes, we apply the density distributions obtained within the generator coordinate method [43]. In Ref. [43] the ^{14}Be nucleus is investigated in the three-cluster GCM, involving several $^{12}\text{Be}+n+n$ configurations. The ^{12}Be core nucleus is described in the harmonic-oscillator model with all possible configurations in the p shell. For the ^{12}Be density we use also the one obtained in the framework of the variational Monte Carlo model [55]. In our case, within the VMC method the proton and neutron densities have been computed with the AV18+UX Hamiltonian, in which the Argonne v18 two-nucleon and Urbana X three-nucleon potentials are used [55]. Urbana X is intermediate between the Urbana IX and Illinois-7 models (the latter was used by us in Ref. [7] for the densities of ^{10}Be nucleus).

Complimentary to both microscopic densities of the neutron-rich $^{12,14}\text{Be}$ isotopes, a phenomenological density distribution in the form of the symmetrized Fermi

function (SF) is applied for them:

$$\rho_{SF}(r) = \rho_0 \frac{\sinh(R/a)}{\cosh(R/a) + \cosh(r/a)}, \quad (6)$$

where

$$\rho_0 = \frac{A}{(4\pi R^3/3)} \left[1 + \left(\frac{\pi a}{R} \right)^2 \right]^{-1}. \quad (7)$$

The SF density parameters, the radius R and the diffuseness a in Eq. (6), have been determined in Ref. [21] by fitting (within the Glauber approach) to the experimental cross section data of the $^{12,14}\text{Be}+p$ elastic scattering at 700 MeV. In our calculations we adopt their values, namely $R = 1.37$ fm, $a = 0.67$ fm for ^{12}Be and $R = 0.99$ fm, $a = 0.84$ fm for ^{14}Be . Here we would like to note the bigger diffuseness parameter a in the case of ^{14}Be nucleus, which supports the existence of a halo structure in it. The same SF form with radius and diffuseness parameters 2.275 fm and 0.393 fm was taken for the density of ^{12}C target nucleus when calculating the OPs for $^{12,14}\text{Be}+^{12}\text{C}$ quasielastic scattering.

Additionally, we apply a modified SF density of ^{12}C

$$\rho(r) = \rho_{SF}(r) + \rho_{SF}^{(1)}(r), \quad (8)$$

where the surface effects are revealed through the term $\rho_{SF}^{(1)}(r)$ being the first derivative of $\rho_{SF}(r)$. The parameters of this density were obtained in Ref. [65] by fitting to electron-nucleus scattering data. In general, the form (8) of the density distribution has a specific bump near the nuclear surface, where the elastic process is expected mainly to take place.

As can be seen from Fig. 1, the proton densities are very similar in ^{12}Be and ^{14}Be nuclei. On the contrary, neutron densities are quite different: whereas neutron density in ^{12}Be is nearly proportional to the proton density, the neutron contribution in ^{14}Be has a very long tail. This long-range neutron density is typical for neutron-rich halo nuclei and yields fairly large rms radii (value of 2.95 fm obtained in GCM was reported in Ref. [43]). One can observe also from Fig. 1 a different behavior of the point-neutron densities of ^{12}Be calculated with GCM and VMC method. In the GCM the ^{12}Be internal wave functions are defined in the p -shell harmonic-oscillator model that leads to a more steep decrease of the corresponding density [43]. On the contrary, the VMC neutron density exhibits a broader shape, presumably due to the ^{10}Be core plus $2n$ cluster structure effectively accounted for in the variational calculations [55]. Similar behavior of the proton and neutron densities of ^{10}Be and ^{11}Be nuclei obtained in the GCM and in the quantum Monte Carlo method can be seen from Fig. 1 of Ref. [7]. As a result from these differences in the surface region, the neutron rms radius r_n of ^{12}Be obtained within the VMC method has a value of 2.60 fm that is larger than the corresponding value of r_n deduced from the GCM (2.33 fm).

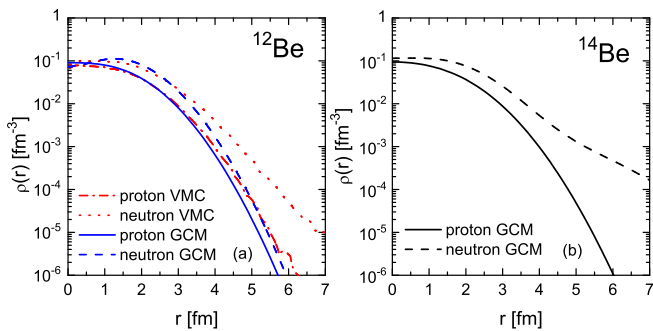


FIG. 1. (a) Point-proton (normalized to $Z = 4$) and point-neutron (normalized to $N = 8$) densities of ^{12}Be obtained in the VMC method and in the GCM; (b) Point-proton (normalized to $Z = 4$) and point-neutron (normalized to $N = 10$) densities of ^{14}Be obtained in the GCM.

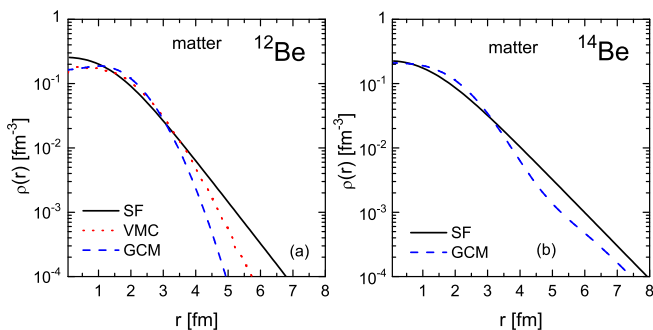


FIG. 2. (a) Matter density distribution (normalized to $A = 12$) of ^{12}Be obtained with SF function, in the VMC method and in the GCM; (b) Matter density distribution (normalized to $A = 14$) of ^{14}Be obtained with SF function and in the GCM.

In Fig. 2 we present the matter density distributions in ^{12}Be and ^{14}Be nuclei. As can be seen, the SF matter density of ^{12}Be exceeds the VMC and GCM densities in the central region ($r < 1.5$ fm), while in the region $2 < r < 3$ fm its values are smaller than the ones of the two microscopic densities, which signals for a mixed p - sd state for the valence neutrons in ^{12}Be [21]. Also, the SF matter density of ^{12}Be indicates an extended tail in comparison with VMC and GCM densities. It was mentioned in Ref. [21] that there is a tendency for a slightly larger rms matter radius, as compared to those obtained in previous measurements. In addition, the relatively big diffuseness parameter $a = 0.67$ fm obtained for the SF model leads to the enhanced matter distribution in the ^{12}Be nucleus.

The values of the rms radii of the point-proton, point-neutron, and matter distributions of $^{12,14}\text{Be}$ used in our calculations are listed in Table I together with the experimental data deduced from the Glauber analysis of the interaction and reaction cross sections [15]. In addition, the values of the matter rms radii of ^{12}Be and ^{14}Be nuclei of SF distributions shown in Fig. 2 are 2.71 fm and 3.22 fm, correspondingly [21].

TABLE I. Proton, neutron, and matter rms radii (in fm) of ^{12}Be and ^{14}Be nuclei obtained within the VMC method [55] and GCM [43]. Experimental data are taken from Ref. [15].

Nucleus	Model	r_p	r_n	r_m
^{12}Be	VMC	2.29	2.60	2.50
	GCM	2.20	2.33	2.29
	Exp. [15]	2.49	2.65	2.59
^{14}Be	GCM	2.28	2.95	2.78
	Exp. [15]	3.00	3.22	3.16

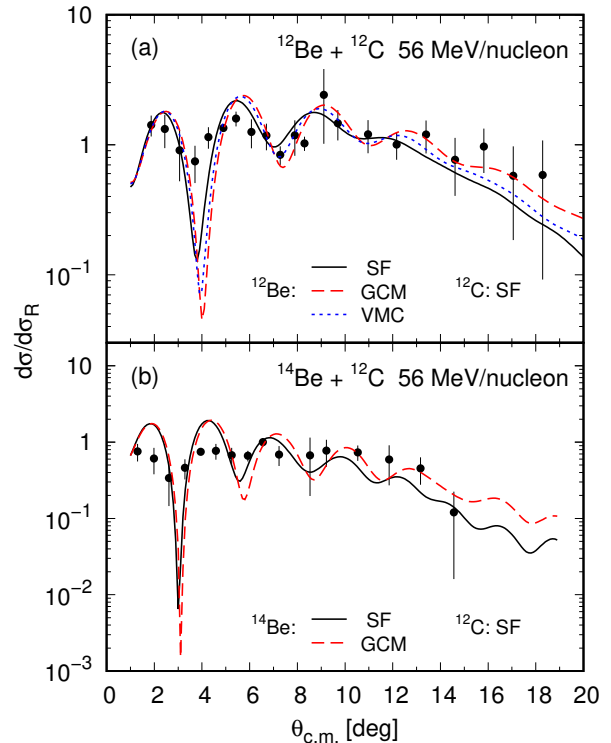


FIG. 3. $^{12}\text{Be}+^{12}\text{C}$ (a) and $^{14}\text{Be}+^{12}\text{C}$ (b) at $E = 56$ MeV/nucleon elastic scattering cross sections. Black solid line: calculations with the SF densities of $^{12,14}\text{Be}$; red dashed line: calculations with the GCM densities of $^{12,14}\text{Be}$; blue dotted line: calculations with the VMC density of ^{12}Be . Experimental data are taken from Ref. [46].

1. Quasielastic scattering cross sections of $^{12,14}\text{Be}+^{12}\text{C}$

Similarly to our previous works (for instance, Ref. [8]), we consider the set of the N_i coefficients (N_R and N_I , see Eq. (1) for the OP) as parameters to be found out from the fit to the experimental data for the cross sections using the χ^2 -procedure. The fitted N_s related to the depths of the ReOP and ImOP can be considered as a measure of deviations of our microscopic OPs from the case when the values of N_s are equal to unity.

It is worth to mention that the experimental data of $^{12,14}\text{Be}$ scattering on ^{12}C [46, 47] are considered to include contributions of the scattering to the first excited

2^+ (4.439 MeV) and 3^- (9.641 MeV) states of ^{12}C . Therefore, to calculate the angular distributions and to compare them with the experimental data we write the following sum:

$$\left(\frac{d\sigma}{d\sigma_R}\right)_{quasi} = \left(\frac{d\sigma}{d\sigma_R}\right)_{el} + C \left(\frac{d\sigma}{d\sigma_R}\right)_{inel}, \quad (9)$$

where the first term corresponds to the pure elastic scattering, while the second term gives the contribution of the inelastic scattering to the 2^+ and 3^- states of ^{12}C . The account for the latter states is important since the coupling between 2^+ state and the ground state of ^{12}C is strong. In Eq. (9) the coefficient C , which is an additional fitting parameter, is related with the potential radius R_{pot} and the deformation parameter β as $C = (\beta R_{pot})^2$. We adopt $R_{pot} = 4.25$ fm as in Ref. [46]. Then, the value of the parameter β can be determined. Concerning the contribution of the inelastic channel, the inelastic OP is calculated within our approach via the microscopic optical potential (1): $U_{inel}(r) = -R_{pot}[dU(r)/dr]$.

First, before estimating the role of the inelastic channels in the scattering process it is useful to perform calculations of the elastic scattering only. The calculated within the hybrid model elastic scattering cross sections of $^{12}\text{Be}+^{12}\text{C}$ and $^{14}\text{Be}+^{12}\text{C}$ at energy $E = 56$ MeV/nucleon in the laboratory frame are given in Fig. 3 and compared with the experimental data [46]. It can be seen in the case of the $^{12}\text{Be}+^{12}\text{C}$ scattering that, with the exception of the deep first minimum, all three SF, GCM, and VMC densities of ^{12}Be give a reasonable agreement with the data. In the case of $^{14}\text{Be}+^{12}\text{C}$, however, an agreement can be seen only at $\theta_{c.m.} > 5^\circ$.

Here we note that the experimental data given in Refs. [46, 47] are presented by the authors as quasielastic cross sections, in which there are contributions of elastic and also of inelastic scattering with an excitation of low-lying 2^+ and 3^- states of ^{12}C nucleus. In Fig. 4 we give the cross section for the quasielastic $^{12}\text{Be}+^{12}\text{C}$ process using only the SF density and including the contribution of the inelastic scattering to first 2^+ and 3^- states. It can be seen that the account for the inelastic scattering reduces the depth of the first minimum and provides the left-shift correction of its place. We note that the role of the scattering to the 3^- state turns out to be negligible. The similar qualities of the results can be seen in Fig. 5 where the quasielastic cross sections calculated with the SF, GCM, and VMC densities of ^{12}Be for the $^{12}\text{Be}+^{12}\text{C}$ case and with SF and GCM densities of ^{14}Be for the $^{14}\text{Be}+^{12}\text{C}$ case are considered.

In the upper part of Fig. 6 we present the quasielastic cross section for the $^{12}\text{Be}+^{12}\text{C}$ case using the SF density of ^{12}Be with excitation of 2^+ and 3^- states of ^{12}C and also including the surface part ($\rho_{SF}^{(1)}$) of the ^{12}C density. The latter leads to a further decrease of the depth of the first minimum. As can be seen in the lower part of Fig. 6 the situation is similar also in the cases of GCM and VMC densities of ^{12}Be . In our opinion, the use of the SF density gives a better agreement with the data.

The results of the calculations in the case of $^{14}\text{Be}+^{12}\text{C}$ at 56 MeV/nucleon given in Fig. 7 show that the account for the surface part ($\rho_{SF}^{(1)}$) of the ^{12}C density does not improve the agreement of the quasielastic scattering at angles $\theta_{c.m.} < 5^\circ$ for both SF and GCM densities. As can be seen from Figs. 4-7 a better agreement with the data (in the case of $^{12}\text{Be}+^{12}\text{C}$) up to 8° is obtained by accounting only for the elastic channel, while for larger angles up to 17° the contributions of the elastic and inelastic scattering (with an excitation mainly of the 2^+ state) are similar in their magnitude and their sum gives an agreement with the data.

The obtained values of the parameters N_R , N_I , the deformation parameter β_{2^+} , and the total reaction cross section σ_R for the $^{12,14}\text{Be}+^{12}\text{C}$ quasielastic scattering at 56 MeV/nucleon incident energy are presented in Table II for the different densities, for the pure elastic channel, also when the inelastic channels are included, and when the surface part of the target ^{12}C density is accounted for. It can be seen from Table II that our "best fit" results to the experimental angular distributions using microscopic OPs lead to values of the predicted total reaction cross sections σ_R occupying an intermediate region between the respective values (discussed in the Introduction) from the analyses of the data in Refs. [46] and [47].

2. Elastic scattering cross sections of $^{12,14}\text{Be}+p$

In Fig. 8 we present, in comparison with the experimental data from [21], our results of calculations for the cross sections of $^{12}\text{Be}+p$ scattering at $E = 703.5$ MeV/nucleon (upper panel) and of $^{14}\text{Be}+p$ at $E = 702.9$ MeV/nucleon (lower panel) using SF, GCM, and VMC densities in the former case and SF and GCM densities in the latter case.

As shown in [66, 67], the effects of relativization are very important at these energies. Here in calculating differential cross sections the respective optical potentials (5) are used dependent on the relativistic velocity $v = k/\sqrt{k^2 + m^2}$ ($c = 1$) for high energies. For our purposes the DWUCK4 code [64] was adapted for relativistic energies to solve the relativistic wave equation at kinetic energies $T \gg |U^H|$ (below $\hbar=c=1$):

$$(\Delta + k^2) \psi(\mathbf{r}) = 2\bar{\mu}U(r)\psi(\mathbf{r}), \quad U = U^H + U_C. \quad (10)$$

In Eq. (10) k is the relativistic momentum of a nucleon in center-of-mass (c.m.) system,

$$k = \frac{Mk^{lab}}{\sqrt{(M+m)^2 + 2MT^{lab}}}, \quad k^{lab} = \sqrt{T^{lab}(T^{lab} + 2m)}, \quad (11)$$

$\bar{\mu} = EM/(E + M)$ is the relativistic reduced mass with $E = \sqrt{k^2 + m^2}$ being the total energy in c.m. system, T^{lab} is the kinetic energy, m and M are the nucleon and nucleus masses.

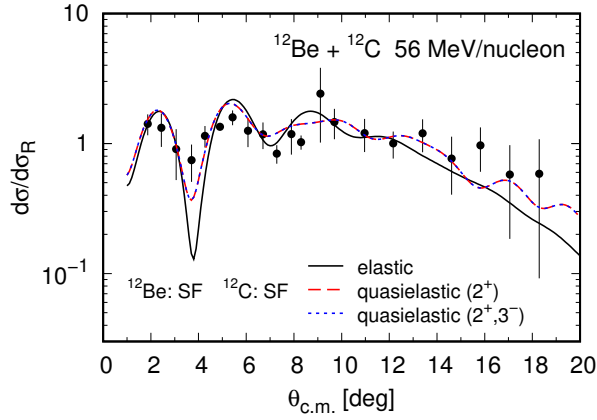


FIG. 4. $^{12}\text{Be}+^{12}\text{C}$ quasielastic scattering cross sections at $E = 56$ MeV/nucleon calculated using the SF density of ^{12}Be . Black solid line: pure elastic scattering; red dashed line: elastic plus inelastic scattering to the 2^+ state of ^{12}C ; blue dotted line: elastic plus inelastic scattering to the first 2^+ and 3^- states of ^{12}C . Experimental data are taken from Ref. [46].

In Ref. [67] the $^{12,14}\text{Be}+p$ cross sections at 700 MeV/nucleon were calculated by using the NN amplitude parameters $\bar{\sigma}_N$ and \bar{a} from Ref. [21], and they reasonably reproduce the experimental data. In this work, to improve the agreement with the data [21], the respective parameters $\bar{\sigma}_N$ and \bar{a} of the optical potential (5) were fitted to the data and the obtained results are presented in Table III. The value of $\bar{\beta} = 0.17$ fm 2 from Ref. [21] was used.

It can be seen from Fig. 8 that for $^{12}\text{Be}+p$ scattering the tested VMC density provides a reasonable agreement with all the data, and the GSM density is consistent with the data only at $\theta < 8^\circ$, while in the case of SF density one gets good fit of the data at all angles of scattering. In the case of ^{14}Be one obtains the remarkable accordance with the data for the SF density, while in the case of GCM density a considerable excess of the data at $\theta > 7^\circ$ is seen.

III. BREAKUP REACTIONS OF ^{14}Be

Along with the small separation energy of one- or two-neutrons (protons) and a large rms radius of the corresponding density distribution, the narrow momentum distributions of the fragments in the breakup of a given nucleus is a proof of a largely extended distribution. In our previous works we calculated the breakup cross sections and momentum distributions of the cluster fragments in the scattering of ^{11}Li on protons at 62 MeV/nucleon [6], of ^{11}Be on ^9Be , ^{93}Nb , ^{181}Ta , and ^{238}U [7], as well as of ^8B on ^9Be , ^{12}C , and ^{197}Au targets [8]. A cluster model, in which the nucleus consists of a halo and a core, has been used in the calculations. In the present section we calculate the breakup cross sections and momentum distributions of ^{12}Be fragments from the

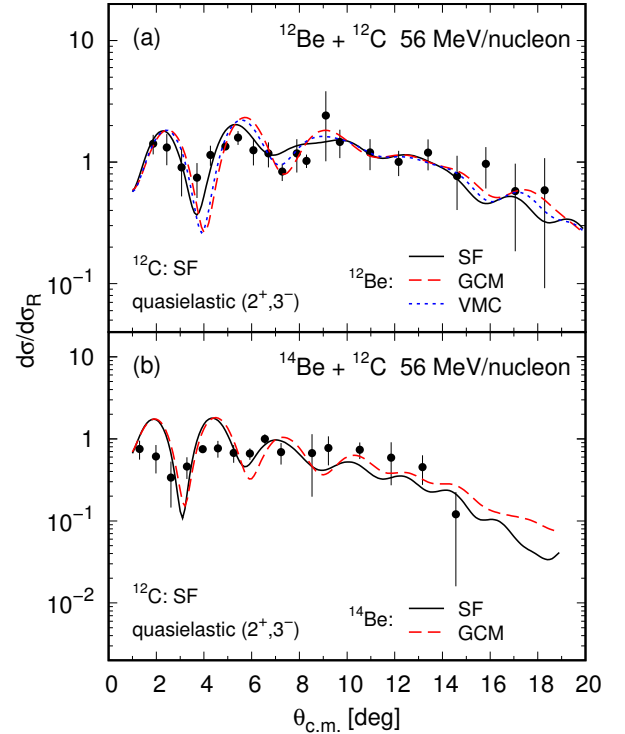


FIG. 5. The same as in Fig. 3 but for the quasielastic scattering cross sections accounting for inelastic scattering to the first 2^+ and 3^- states in ^{12}C .

TABLE II. The renormalization parameters N_R , N_I , the deformation parameter β_{2+} , and the total reaction cross sections σ_R (in mb) for results of the $^{12,14}\text{Be}+^{12}\text{C}$ quasielastic scattering processes at 56 MeV/nucleon incident energy considered and shown in Figs. 3–7 using different model densities of $^{12,14}\text{Be}$ and ^{12}C (for details, see the text).

Nucleus	Model $^{12,14}\text{Be}$	Model ^{12}C	N_R	N_I	β_{2+}	σ_R
^{12}Be elastic	SF	SF	0.767	0.593		1124.80
	GCM		0.804	0.855		1018.47
	VMC		0.721	0.660		1055.15
quasielastic	SF		0.702	1.294	0.635	1353.04
	GCM		0.496	1.431	0.437	1111.34
	VMC		0.583	1.156	0.487	1180.38
	SF	mod. SF	0.647	1.094	0.665	1422.01
	GCM		0.592	1.133	0.526	1228.79
	VMC		0.596	1.106	0.593	1309.78
^{14}Be elastic	SF	SF	0.913	1.310		1666.02
	GCM		1.080	2.000		1597.48
quasielastic	SF		0.701	1.252	0.365	1636.39
	GCM		0.638	2.000	0.375	1583.53
	SF	mod. SF	0.599	0.952	0.362	1629.13
	GCM		0.708	1.920	0.369	1701.64

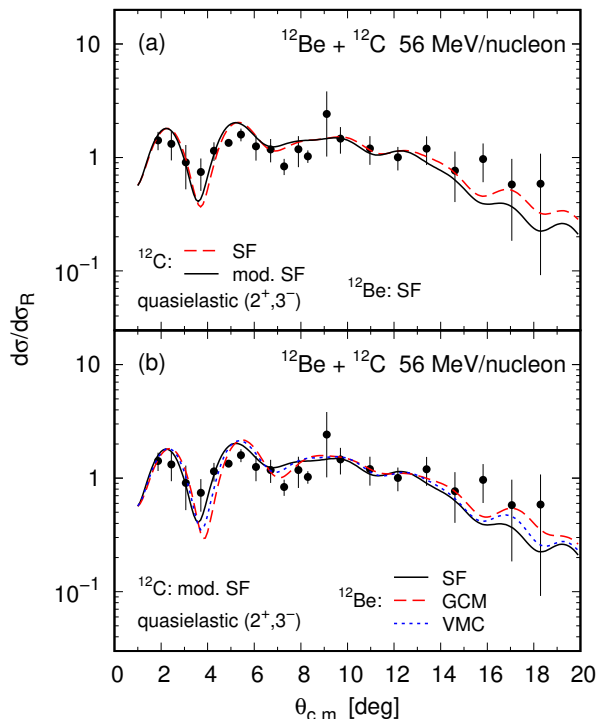


FIG. 6. (a) $^{12}\text{Be}+^{12}\text{C}$ quasielastic scattering cross sections at $E = 56$ MeV/nucleon calculated using the SF density of ^{12}Be and SF [Eq. (6)] (black solid line) and modified SF [Eq. (8)] (red dashed line) densities of ^{12}C ; The panel (b) illustrates the calculations with the modified SF density of ^{12}C [Eq. (8)] and using the SF (black solid line), GCM (red dashed line), and VMC (blue dotted line) densities of ^{12}Be .

TABLE III. Parameters $\bar{\sigma}_N$ (in fm^2), $\bar{\alpha}$, and the total reaction cross sections σ_R (in mb) for results of the $^{12,14}\text{Be}+p$ elastic scattering processes at incident energies $E = 702.9$ and $E = 703.5$ MeV/nucleon considered and shown in Fig. 8 using different model densities of $^{12,14}\text{Be}$.

Nucleus	E/A	Model	$\bar{\sigma}_N$	$\bar{\alpha}$	σ_R
^{12}Be	703.5	SF	4.4	-0.237	278.49
		GCM	3.5	-0.483	219.02
		VMC	3.8	-0.416	246.18
^{14}Be	702.9	SF	4.136	-0.2086	333.19
		GCM	3.46	-0.35	270.24

breakup of the halo-nucleus ^{14}Be on ^{12}C at energy 56.8 MeV/nucleon [16]. This part of the work is related to the already mentioned in the Introduction general question about the behavior of dineutron formations in exotic nuclei predicted theoretically in Ref. [20] and considered also, e.g., in Refs. [21–26]), as well as to the results of the experiments on dineutron decay of ^{16}Be and its properties observed in Ref. [27].

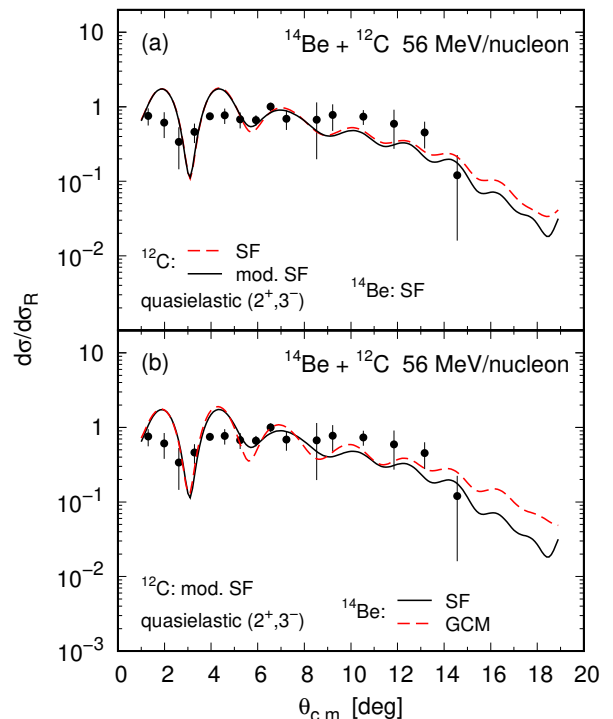


FIG. 7. The same as in Fig. 6 but for the $^{14}\text{Be}+^{12}\text{C}$ quasielastic scattering cross sections at $E = 56$ MeV/nucleon. In panel (b) results with SF and GCM densities of ^{14}Be are shown.

A. The $^{12}\text{Be}+2n$ model of ^{14}Be

We consider the characteristics of breakup processes of ^{14}Be nucleus, namely diffraction and stripping reaction cross sections and momentum distributions of the fragments. A simple cluster model in which ^{14}Be consists of ^{12}Be core and a valence $2n$ -halo is used. In this case the hybrid model is applied to calculate the OPs of the interactions of ^{12}Be and $2n$ with the target. The sum of OPs is folded with the density distribution which corresponds to the wave function of the relative motion of the clusters in ^{14}Be . This wave function is obtained as a solution of the Schrödinger wave equation with the WS potential for a particle with a reduced mass of the two clusters. The values of the parameters of the WS potentials are obtained by a fitting procedure to reach the empirical two-neutron separation energy S_{2n} of the dineutron halo and the rms radius R_{rms} corresponding to the cluster wave function.

The eikonal formalism for the S -matrix as a function of the impact parameter b is used to calculate the breakup cross sections and momentum distributions of fragments:

$$S(b) = \exp \left[-\frac{i}{\hbar v} \int_{-\infty}^{\infty} U(\sqrt{b^2 + z^2}) dz \right], \quad (12)$$

where

$$U = V + iW \quad (13)$$

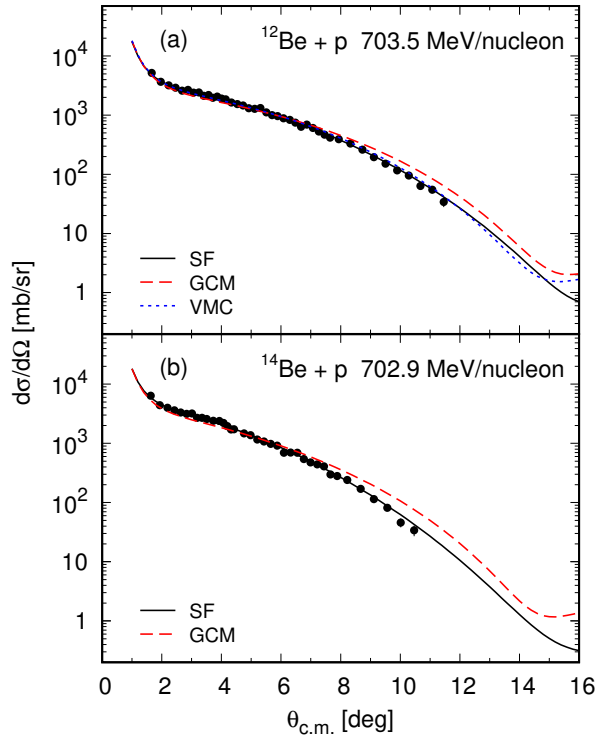


FIG. 8. Differential cross sections for $^{12}\text{Be}+p$ at $E = 703.5$ MeV/nucleon (a) and $^{14}\text{Be}+p$ at $E = 702.9$ MeV/nucleon (b) elastic scattering. Calculations are performed with the modified SF density of ^{12}C [Eq. (8)] and different densities of $^{12,14}\text{Be}$. Black solid line: calculations with the SF densities of $^{12,14}\text{Be}$; red dashed line: calculations with the GCM densities of $^{12,14}\text{Be}$; blue dotted line: calculations with the VMC density of ^{12}Be . Experimental data are taken from Ref. [21].

$$\frac{d\sigma}{dk_{\parallel}dk_{\perp}} = \frac{1}{2l+1} \frac{4k_{\perp}}{k^2} \int d^2b \sum_{M,m} \left| \int dr \int d(\cos\theta) \sum_L (-i)^L u_{k,L}(r) g_l(r) \tilde{Y}_{L,M}(\theta_k) \tilde{Y}_{L,M}^*(\theta) \tilde{Y}_{l,m}(\theta) \right. \\ \left. \times \int d\varphi \exp(i(m-M)\varphi) S_c(\mathbf{b}_c) S_v(\mathbf{b}_v) \right|^2, \quad (15)$$

where \mathbf{k} is the relative momentum of both clusters in their c.m. frame and k_{\parallel} and k_{\perp} are its parallel and transverse components. The relative motion wave function of the fragments of $a = c + v$ in the continuous final state was taken as

$$\phi_{\mathbf{k}}(\mathbf{r}) = 4\pi \sum_{L,M} i^L \frac{u_{k,L}(r)}{kr} Y_{LM}(\hat{r}) Y_{LM}^*(\hat{k}), \quad (16)$$

where in the further estimations we neglect the distortion effect and thus use $u_{k,L}(r) = kr j_L(kr)$. Also, $g_l(r)$ is the radial part of the initial bound state wave function of the clusters c and v and $Y_{LM}(\hat{k}) = \tilde{Y}_{L,M}(\theta_k) \exp(iM\varphi_k)$.

In the case of the s -state for the mutual motion of the clusters in the incident nucleus $a = c + v$ the cross sections

is the OP. The probability that after the collision with the target ($z \rightarrow \infty$) the core (c) or the valence halo ($v = 2n$) with impact parameter b remains in the elastic channel ($i = c, v$) is given by:

$$|S_i(b)|^2 = \exp \left[-\frac{2}{\hbar v} \int_{-\infty}^{\infty} dz \left| W_i(\sqrt{b^2 + z^2}) \right| \right]. \quad (14)$$

The probability of a cluster to be removed from the elastic channel is $(1 - |S_i|^2)$. The probability both clusters (c and v) to leave the elastic channel is $(1 - |S_c|^2)(1 - |S_v|^2)$. We note that this procedure can lead to several groups of parameters of the OPs which fulfill the conditions. They can be similar, but at the same time to lead to different values of the rms radius of the $2n$ -cluster (the distance between ^{12}Be and $2n$ in the case of ^{14}Be). In our calculations we use different values of the rms radii corresponding to the cluster wave functions, like what has been done in our work on ^8B breakup processes (see Ref. [8], Table 4), where we used three values of the relative distances in the system of ^7Be and p clusters.

For the cross section of the breakup of the incident nucleus (a) into two clusters ($a + A \rightarrow c + v + A$) we use, following Ref. [68], the form:

of the stripping reaction when the valence cluster $v = 2n$ leaves the elastic channel is:

$$\left(\frac{d\sigma}{dk_{\parallel}} \right)_{\text{str}} = \frac{1}{2\pi^2} \int d^2b_v [1 - |S_v(b_v)|^2] \int d^2\rho |S_c(b_c)|^2 \\ \times \left[\int dz \cos(k_{\parallel}z) \phi_0(\sqrt{\rho^2 + z^2}) \right]^2, \quad (17)$$

with $\mathbf{r} = \rho + \mathbf{z}$ and $\rho = \mathbf{b}_v - \mathbf{b}_c$.

B. Results of calculations of breakup reactions

The results of our calculations of the ^{12}Be longitudinal momentum distribution from ^{14}Be fragmentation on ^{12}C

at incident energy of 56.8 MeV/nucleon for stripping and diffraction processes are given in Figs. 9 and 10, correspondingly. In both figures they are compared with the experimental data taken from Fig. 3(a) of Ref. [16] (obtained there via the telescope method). In order to check the sensitivity of the results towards the value of the rms radius corresponding to the wave function of the relative motion of the clusters in ^{14}Be , in each of the figures we present two theoretical curves. They illustrate the results for rms radii $R_{rms} = 3.10$ fm and $R_{rms} = 3.50$ fm which are related to possible estimated limits of the values of rms radius of ^{14}Be , namely, when using its total SF density ($r_m = 3.22$ fm) and also by estimations on the base of the values of the rms radius of the core ^{12}Be of 2.8 fm [1, 16] and a rms halo radius of ^{14}Be of about 5.5 fm [1] (both taken from Ref. [16]). The weighted mean rms matter radius of ^{14}Be deduced in Ref. [21] from several one-body density parametrizations that are obtained by fitting the experimental $p+^{14}\text{Be}$ elastic scattering cross sections is 3.25(11) fm.

As can be seen, the theoretical results for the stripping and diffractive processes have a similar shape. This is expected for the energies considered in our work having in mind the results obtained in Ref. [68] (see also Refs. [69–72]) for energies up to 100 MeV/nucleon.

The obtained values of the widths are 80.2 MeV/c and 77.8 MeV/c with $R_{rms} = 3.10$ fm and $R_{rms} = 3.50$ fm, correspondingly, for the stripping reaction, and 115.7 MeV/c and 112.7 MeV/c for the same values of radii in the case of diffraction process. These values are in a reasonable agreement with the experimental width ($\Gamma = 92.2 \pm 2.7$ MeV/c) estimated in Ref. [16]. A quite weak dependence of the width at a given energy on the choice of the rms radius was found. It turns out that the main condition for the width to have a correct value is the parameters of the potential well (e.g., of Woods-Saxon type) to provide the right value of the binding energy of the pair of neutrons in the ^{14}Be nucleus. In our calculations the parameter values of the Woods-Saxon potential are: $V_0 = 20.6$ MeV, $r_0 = 2.7$ fm, $a_0 = 0.30$ fm for $R_{rms} = 3.10$ fm and $V_0 = 16.8$ MeV, $r_0 = 3.0$ fm, $a_0 = 0.40$ fm for $R_{rms} = 3.50$ fm.

IV. CONCLUSIONS

In the present work we followed two main aims. The first one was to study elastic and quasielastic scattering of the neutron-rich exotic nuclei ^{12}Be and ^{14}Be on ^{12}C target at energy 56 MeV/nucleon, as well as their scattering on protons at 703.5 and 702.9 MeV/nucleon, correspondingly. The second aim was to calculate the longitudinal momentum distribution of ^{12}Be from the fragmentation of ^{14}Be on ^{12}C at incident energy 56.8 MeV/nucleon.

In our hybrid model we calculate the real part of the optical potential microscopically by the folding procedure in which microscopic densities GCM and VMC for ^{12}Be and GCM for ^{14}Be nucleus, as well as the sym-

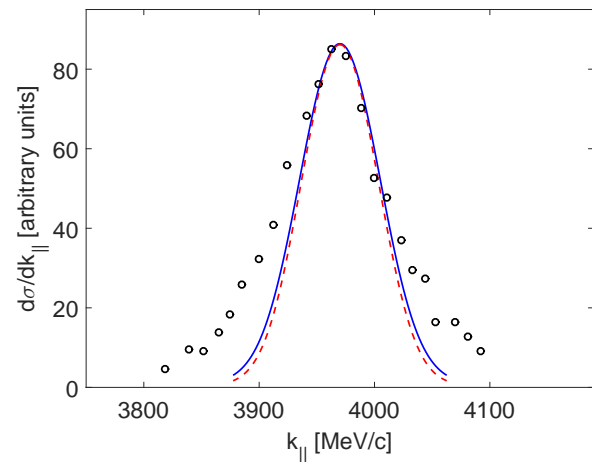


FIG. 9. Cross sections of stripping reaction in $^{14}\text{Be}+^{12}\text{C}$ scattering at 56.8 MeV/nucleon. Blue solid line: result with rms radius $R_{rms} = 3.10$ fm, red dashed line: result with rms radius $R_{rms} = 3.50$ fm. Experimental data are taken from Fig 3(a) of Ref. [16].

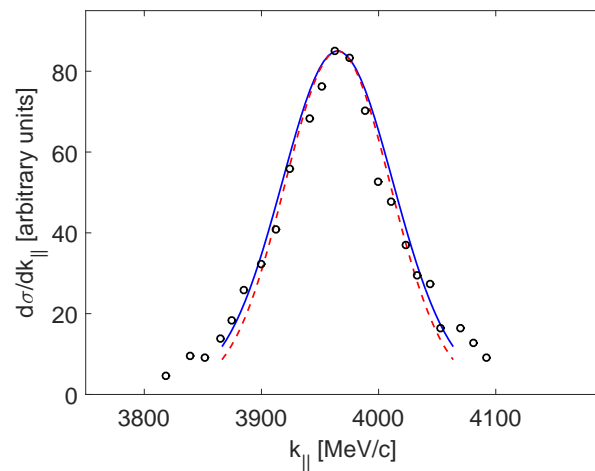


FIG. 10. Cross sections of diffraction breakup reaction in $^{14}\text{Be}+^{12}\text{C}$ scattering at 56.8 MeV/nucleon. Blue solid line: result with rms radius $R_{rms} = 3.10$ fm, red dashed line: result with rms radius $R_{rms} = 3.50$ fm. Experimental data are taken from Fig 3(a) of Ref. [16].

metrized Fermi density (SF) for both nuclei were used. Another ingredient of the folding procedure is the effective NN interaction related to the g -matrix obtained on the basis of the Paris NN potential. The ReOP includes isoscalar and isovector direct and exchange components. The ImOP is calculated microscopically as the folding OP that reproduces the phase of the scattering in the high-energy approximation. The free parameters of the model are the depths of the real and imaginary parts of the OP. Their values are obtained by fitting the experimental data on differential cross sections. We calculated also the contributions of inelastic scattering to the first 2^+ and 3^- excited states in ^{12}C in the quasielastic $^{12,14}\text{Be} + ^{12}\text{C}$ processes. In addition, we studied the role of the

surface part $\rho_{SF}^{(1)}$ of the density of the ^{12}C target.

The main results from the work can be summarized as follows:

(i) In the case of the quasielastic $^{12}\text{Be}+^{12}\text{C}$ scattering all three densities of ^{12}Be (SF, GCM, and VMC) give a reasonable agreement with the data with the exception of the depth and the position of the first minimum when only the elastic channel is included. In the case of $^{14}\text{Be}+^{12}\text{C}$ an agreement can be seen only at $\theta_{c.m.} > 5^\circ$.

(ii) The account for the contribution of inelastic scattering to the first 2^+ state improves the depth of the first minimum and leads to a left-shift correction of its place for both processes. We note that a better agreement with the data for the $^{12}\text{Be}+^{12}\text{C}$ case for $\theta_{c.m.} < 8^\circ$ is obtained by accounting only for the elastic scattering, while for larger angles up to 17° the elastic and inelastic scattering (to the 2^+ state) give similar contributions and their sum allows a reasonable agreement with the experimental data to be obtained.

(iii) The inclusion of the surface part $\rho_{SF}^{(1)}$ of the ^{12}C density leads to a correct reduction of the depth of the first minimum and a good overall agreement with the data for the $^{12}\text{Be}+^{12}\text{C}$ case is achieved. However, for $^{14}\text{Be}+^{12}\text{C}$ this does not improve the agreement at angles $\theta_{c.m.} < 5^\circ$.

(iv) A good agreement with the experimental $^{12}\text{Be}+p$ data for the differential cross sections at 703.5 MeV/nucleon in the whole range of angles is obtained with the use of SF and VMC densities of ^{12}Be . The use of SF density of ^{14}Be leads also to a very good agreement with the experimental $^{14}\text{Be}+p$ cross sections data at 702.9 MeV/nucleon. The successful description of both elastic scattering processes proves the important role of the effects of relativization included in the calculations.

(v) In the second part of the work the longitudinal momentum distribution of fragments in stripping and diffractive breakup processes of ^{14}Be nucleus on ^{12}C is calculated in a cluster model in which ^{14}Be consists of ^{12}Be core and a $2n$ halo. OPs of the interactions of ^{12}Be

and $2n$ with the target are calculated within our hybrid model and their sum is used in the folding procedure with the density corresponding to the wave function of the relative motion of the clusters in ^{14}Be . Using the cluster OPs the corresponding core (c) and valence halo ($v = 2n$) functions S_c and S_v (matrices) are obtained within the eikonal formalism. They are used to calculate the longitudinal momentum distributions of ^{12}Be fragments produced in the breakup of the halo-nucleus $^{14}\text{Be}+^{12}\text{C}$ at energy 56.8 MeV/nucleon. The obtained widths are in a reasonable agreement with the experimental data and give an important information for the halo structure of these nuclei. A quite weak sensitivity of the computed widths to the choice of the rms radius of ^{14}Be was found.

In general, we can conclude that our microscopic approach applied to reaction studies with neutron-rich $^{12,14}\text{Be}$ nuclei is capable to reproduce the existing experimental data and allows to support the two-neutron halo interpretation of these nuclei. More definite conclusions about the relative role of the theoretical ingredients of the microscopic model could be drawn when complete and precise data from new reactions measurements, e.g., with the novel generation of radioactive nuclear beam facilities, will become available.

V. ACKNOWLEDGMENTS

The authors are grateful to S. C. Pieper for providing with the density distributions of ^{12}Be nucleus calculated within the VMC method and to P. Descouvemont for the density distributions of $^{12,14}\text{Be}$ nuclei obtained within the GCM. The authors thank J. J. Kolata for the discussion. Three of the authors (V.K.L., E.V.Z. and K.V.L.) thank the Russian Foundation for Basic Research (Grant No. 17-52-18057 bolg-a) for the partial support. D.N.K., A.N.A., and M.K.G. are grateful for the support of the Bulgarian Science Fund under Contracts No. DFNI-T02/19 and No. DNTS/Russia 01/3.

-
- [1] I. Tanihata, H. Hamagaki, O. Hashimoto, Y. Shida, N. Yoshikawa, K. Sugimoto, O. Yamakawa, T. Kobayashi, and N. Takahashi, Phys. Rev. Lett. **55**, 2676 (1985).
 - [2] I. Tanihata, H. Hamagaki, O. Hashimoto, S. Nagamiya, Y. Shida, N. Yoshikawa, O. Yamakawa, K. Sugimoto, T. Kobayashi, D. E. Greiner, N. Takahashi, and Y. Nojiri, Phys. Lett. B **160**, 380 (1985).
 - [3] K. V. Lukyanov, V. K. Lukyanov, E. V. Zemlyanaya, A. N. Antonov, and M. K. Gaidarov, Eur. Phys. J. A **33**, 389 (2007).
 - [4] V. K. Lukyanov, E. V. Zemlyanaya, K. V. Lukyanov, D. N. Kadrev, A. N. Antonov, M. K. Gaidarov, and S. E. Massen, Phys. Rev. C **80**, 024609 (2009).
 - [5] V. K. Lukyanov, D. N. Kadrev, E. V. Zemlyanaya, A. N. Antonov, K. V. Lukyanov, and M. K. Gaidarov, Phys. Rev. C **82**, 024604 (2010).
 - [6] V. K. Lukyanov, E. V. Zemlyanaya, K. V. Lukyanov, D. N. Kadrev, A. N. Antonov, M. K. Gaidarov, and K. Spasova, Phys. Rev. C **88**, 034612 (2013).
 - [7] V. K. Lukyanov, D. N. Kadrev, E. V. Zemlyanaya, K. Spasova, K. V. Lukyanov, A. N. Antonov, and M. K. Gaidarov, Phys. Rev. C **91**, 034606 (2015).
 - [8] V. K. Lukyanov, D. N. Kadrev, E. V. Zemlyanaya, A. N. Antonov, K. V. Lukyanov, M. K. Gaidarov, and K. Spasova, Eur. Phys. J. A **53**, 31 (2017).
 - [9] H. Iwasaki *et al.*, Phys. Lett. B **481**, 7 (2000).
 - [10] H. Iwasaki *et al.*, Phys. Lett. B **491**, 8 (2000).
 - [11] A. Navin *et al.*, Phys. Rev. Lett. **85**, 266 (2000).
 - [12] S. Shimoura *et al.*, Phys. Lett. B **560**, 31 (2003).
 - [13] S.D. Pain *et al.*, Phys. Rev. Lett. **96**, 032502 (2006).
 - [14] G. Audi, A. H. Wapstra, and C. Thibault, Nucl. Phys. A **729**, 337 (2003).

- [15] I. Tanihata, T. Kobayashi, O. Yamakawa, T. Shimoura, K. Ekuni, K. Sugimoto, N. Takahashi, T. Shimoda, and H. Sato, *Phys. Lett. B* **206**, 592 (1988).
- [16] M. Zahar *et al.*, *Phys. Rev. C* **48**, R1484 (1993).
- [17] T. Suzuki *et al.*, *Nucl. Phys. A* **658**, 313 (1999).
- [18] T. Tarutina, I. J. Thompson, and J. A. Tostevin, *Nucl. Phys. A* **733**, 53 (2004).
- [19] G. Gangopadhyay and Subinit Roy, *J. Phys. G* **31**, 1111 (2005).
- [20] A. B. Migdal, *Yad. Fiz.* **16**, 427 (1972); *Sov. J. Nucl. Phys.* **16**, 238 (1973).
- [21] S. Ilieva *et al.*, *Nucl. Phys. A* **875**, 8 (2012).
- [22] P. G. Hansen and B. Jonson, *Europhys. Lett.* **4**, 409 (1987).
- [23] P. G. Hansen, *Nucl. Phys. A* **553**, 89c (1993).
- [24] T. Otsuka, *Phys. Scripta* **152**, 014007 (2013).
- [25] J. A. Tostevin, R. G. Johnson, and J. S. Al-Khalili, *Nucl. Phys. A* **630**, 340c (1998).
- [26] J. MacDonald and D. J. Mullan, *Phys. Rev. D* **80**, 043507 (2009).
- [27] A. Spirou *et al.*, *Phys. Rev. Lett.* **108**, 102501 (2012).
- [28] Ahmed N. Abdullah, *Int. J. Mod. Phys. E* **26**, 1750048 (2017); *Pramana-J. Phys.* **89**, 43 (2017).
- [29] C. A. Bertulani, L. F. Canto, and M. S. Hussein, *Phys. Rep.* **226**, 281 (1993).
- [30] G. A. Lalazissis, D. Vretenar, and P. Ring, *Eur. Phys. J. A* **22**, 37 (2004).
- [31] E. Liatard *et al.*, *Europhys. Lett.* **13**, 401 (1990).
- [32] Zhongzhou Ren and Gongou Xu, *Phys. Lett. B* **252**, 311 (1990).
- [33] R. A. Radhi, A. K. Hamoudi, and W. Z. Majeed, *Iraqi Journal of Science* **54**, 349 (2013).
- [34] M. T. Yamashita, Lauro Tomio, and T. Frederico, *Nucl. Phys. A* **735**, 40 (2004).
- [35] A. Bhagwat, Y. K. Gambhir, and S. H. Patil, *Eur. Phys. J. A* **8**, 511 (2000); S. Rafi, A. Bhagwat, W. Haider, and Y. K. Gambhir, *Proceedings of the DAE Symp. on Nucl. Phys.* **59**, 326 (2014).
- [36] Bai-Ping Gu and Zhong-Zhou Ren, *Commun. Theor. Phys.* **44**, 337 (2005).
- [37] Zhongzhou Ren, Gongou Xu, Baoqiu Chen, Zhongyu Mad, and W. Mittig, *Phys. Lett. B* **351**, 11 (1995).
- [38] Le Xuan Chung, C. A. Bertulani, P. Egelhof, S. Ilieva, Dao T. Khoa, and O. A. Kiselev, *Phys. Lett. B* **774**, 559 (2017).
- [39] T. Moriguchi *et al.*, *Nucl. Phys. A* **929**, 83 (2014).
- [40] M. Fukuda *et al.*, *EPJ Web of Conferences* **66**, 02037 (2014).
- [41] S. Terashima *et al.*, *Prog. Theor. Exp. Phys.*, 101D02 (2014).
- [42] M. Labiche *et al.*, *Phys. Rev. Lett.* **86**, 600 (2001).
- [43] P. Descouvemont, *Phys. Rev. C* **52**, 704 (1995).
- [44] J. J. Kolata, *Revista Mexicana de Física* **40**, Suplemento 1, 197 (1994).
- [45] P. Banerjee and R. Shyam, *Phys. Lett. B* **349**, 421 (1995).
- [46] M. Zahar *et al.*, *Phys. Rev. C* **49**, 1540 (1994).
- [47] M. C. Mermaz, *Phys. Rev. C* **50**, 2620 (1994).
- [48] M. Aygun, *Journal of the Korean Physical Society* **73**, 1255 (2018).
- [49] Bai-Ping Gu and Zhong-Zhou Ren, *Commun. Theor. Phys.* **46**, 711 (2006).
- [50] V. Durant, P. Capel, L. Huth, A. B. Balantekin, and A. Schwenk, *Phys. Lett. B* **782**, 668 (2018).
- [51] K. V. Lukyanov, E. V. Zemlyanaya, and V. K. Lukyanov, *JINR Preprint P4-2004-115*, Dubna, 2004.
- [52] K. V. Lukyanov, E. V. Zemlyanaya, and V. K. Lukyanov, *Phys. At. Nucl.* **69**, 240 (2006).
- [53] D. T. Khoa and G. R. Satchler, *Nucl. Phys. A* **668**, 3 (2000).
- [54] K. V. Lukyanov, *JINR Comm. R11-2007-38*, Dubna, 2007.
- [55] J. Carlson, S. Gandolfi, F. Pederiva, S. C. Pieper, R. Schiavilla, K. E. Schmidt, and R. B. Wiringa, *Rev. Mod. Phys.* **87**, 1067 (2015); S. C. Pieper, private communication.
- [56] R. J. Glauber, in *Lectures in Theoretical Physics* (New York, Interscience, 1959), p.315.
- [57] A. G. Sitenko, *Ukr. Fiz. J.* **4**, 152 (1959).
- [58] X. Campy and A. Bouyssy, *Phys. Lett. B* **73**, 263 (1978).
- [59] J. W. Negele and D. Vautherin, *Phys. Rev. C* **5**, 1472 (1972).
- [60] P. Shukla, *Phys. Rev. C* **67**, 054607 (2003).
- [61] S. Charagi and G. Gupta, *Phys. Rev. C* **41**, 1610 (1990); **46**, 1982 (1992).
- [62] C. Xiangzhou, F. Jun, S. Wenqing, M. Yugang, W. Jiansong, and Y. Wei, *Phys. Rev. C* **58**, 572 (1998).
- [63] W. Grein, *Nucl. Phys. B* **131**, 255 (1977).
- [64] P. D. Kunz and E. Rost, in *Computational Nuclear Physics*, edited by K. Langanke *et al.* (Springer-Verlag, New York, 1993), Vol. 2, p. 88.
- [65] V. V. Burov, D. N. Kadrev, V. K. Lukyanov, and Yu. S. Pol', *Phys. At. Nucl.* **61**, 525 (1998).
- [66] V. K. Lukyanov, E. V. Zemlyanaya, and K. V. Lukyanov, *Phys. At. Nucl.* **78**, 142 (2015).
- [67] V. K. Lukyanov, E. V. Zemlyanaya, and K. V. Lukyanov, *EPJ Web of Conf.* **204**, 09003 (2019).
- [68] K. Hencken, G. Bertsch, and H. Esbensen, *Phys. Rev. C* **54**, 3043 (1996).
- [69] A. Bonaccorso and D. M. Brink, *Phys. Rev. C* **58**, 2864 (1998).
- [70] T. Aumann *et al.*, *Phys. Rev. Lett.* **84**, 35 (2000).
- [71] K. Yabana, Y. Ogawa, and Y. Suzuki, *Nucl. Phys. A* **539**, 295 (1992).
- [72] R. Anne *et al.*, *Phys. Lett. B* **304**, 55 (1993).